

Inclusion of nonadiabatic effects in calculations on vibrational excitation of molecular hydrogen by low-energy electron impact

S. Mazevet,¹ Michael A. Morrison,^{1,*} Olen Boydston,¹ and R. K. Nesbet²

¹*Department of Physics and Astronomy, The University of Oklahoma, 440 West Brooks Street, Norman, Oklahoma 73019-0225*

²*IBM Almaden Research Center, 650 Harry Road, San Jose, California 95120-6099*

(Received 2 September 1998)

The nonadiabatic phase matrix method offers a unified, systematic treatment of vibrational dynamics in calculations of low-energy inelastic electron-molecule cross sections. This formalism uses fixed-nuclei R matrices to describe the region of configuration space near the target but—unlike its fully adiabatic counterpart, the energy-modified adiabatic method—includes nonadiabatic effects, which are important for resonant scattering and near a vibrational threshold. A most stringent test of this method is e -H₂ scattering below 10 eV, where elastic and inelastic cross sections exhibit an enhancement around 3 eV which at the fixed-nuclei level involves a range of physical effects, from nonresonant to resonant scattering, as the internuclear separation varies from the smallest to largest relevant values. Here we describe an implementation of this method appropriate to such systems, an assessment of its accuracy for e -H₂ scattering, and an appraisal of the importance of nonadiabaticity for the $0 \rightarrow 1$ and $0 \rightarrow 2$ vibrational excitations. [S1050-2947(99)08901-5]

PACS number(s): 34.80.Bm, 34.80.Gs

I. INTRODUCTION

Electron scattering by the hydrogen molecule has been studied extensively by both theorists and experimentalists (for reviews and references, see Refs. [1–3]). Although H₂ is the simplest of all neutral molecular targets, the presence of a fixed-nuclei shape resonance around 3 eV whose width varies drastically with internuclear separation presents a considerable challenge to the theory of vibrational excitation from the ground state [4]. Direct calculation of the ${}^2\Sigma_u$ complex potential-energy function, using quantum chemistry techniques such as the complex self-consistent-field method [5,6], indicate that this resonant state interacts strongly with the electron-scattering continuum for small values of internuclear separation, but becomes bound for internuclear separations around $3a_0$ [7].

This ${}^2\Sigma_u$ resonance enhances inelastic cross sections for excitation to low-lying vibrational states, induces a strong resonant structure in the cross sections for excitation to higher vibrational states [8], and is primarily responsible for dissociative attachment into H and H⁻ [3]. Different theoretical formalisms and computational methods have been used to treat various consequences of this resonance, each adapted to a particular situation. For excitation to low-lying vibrational states, modified adiabatic methods such as the first-order nonadiabatic method [9,10] and the energy-modified adiabatic phase matrix method (EMAP) [11–13], which allow for the transfer of kinetic energy to nuclear motion during an inelastic process but neglect explicitly nonadiabatic effects, are appropriate. However, for deep inelastic scattering or for dissociative attachment, it is expected that a fully nonadiabatic theory such as vibrational close coupling is necessary, in order to describe the relatively strong coupling between electronic and vibrational motion. Due to the diffi-

culty of including continuum channels in a close-coupling formalism, even for e -H₂ scattering, alternative methods such as the projection operator method [3,14,15] have been used. This paper concerns the extension to extremely broad resonances such as the one in the e -H₂ system of an alternative treatment, the nonadiabatic phase matrix (NADP) method [16–18,13].

The NADP method has previously been applied to the narrower resonance structures observed in low-energy e -N₂ scattering [18]. Its advantage for electron-impact vibrational excitation of e -H₂ in the ${}^2\Sigma_u$ symmetry [13] is that this method includes nonadiabatic physics within a formulation which consistently treats the entire range of physical effects that influence e -H₂ cross sections as the internuclear separation R varies, from strongly resonant scattering at large R to purely background scattering at small R .

The NADP method derives this advantage from the use of R matrices to treat the region near the target. (For an alternative R -matrix-based formalism for the inclusion of nonadiabatic effects, see Refs. [19,20].) In a NADP calculation, body-frame fixed-nuclei R matrices are used to define phase matrices at each R . Each phase matrix is decomposed additively into foreground part and background parts. The latter is then converted to a vibronic background phase matrix using the EMAP approximation [21]. Following this methodology, the foreground fixed-nuclei phase matrix is also converted to a foreground vibronic phase matrix by replacing functional forms determined by the electron continuum energy by matrix expressions defined by an operator which explicitly contains the vibrational kinetic-energy operator. The NADP procedure *per se* need be applied only to the resonant symmetry; nonresonant symmetries can be treated with the EMAP method. The case of e -H₂ scattering is particularly appropriate to calibrate this methodology because of the diversity of the effects in ${}^2\Sigma_u$ scattering below 10 eV.

In Sec. II we outline the theoretical foundation of the EMAP and NADP methods and the role of the R matrix in

*Electronic address: MORRISON@MAIL.NHN.OU.EDU

these approximations. Section III is concerned with their implementation for e -H₂ scattering. In Sec. IV we concentrate on tests of the validity of the NADP and EMAP methods for excitation of low-lying vibrational states of H₂. Here we report a systematic comparison of EMAP and NADP total and differential cross sections with benchmark body-frame vibrational close-coupling calculations [22]. To ensure meaningful comparisons among these methods, all calculations use the same Hartree-Fock ground-state H₂ wave function, the same representation of the static, exchange, and correlation polarization terms in the e -H₂ interaction potential, and comparable numerical precision.

II. THEORY

In the continuum Born-Oppenheimer approximation [23], where the vibrational and rotational kinetic energy operators are neglected in equations for the scattering function, the coupled radial integrodifferential equations for an electron scattered by a diatomic molecule, written in the usual body-fixed reference frame with the z axis coincident with the internuclear axis, are [1]

$$\left[\frac{d^2}{dr^2} - \frac{\ell(\ell+1)}{r^2} + k_b^2 \right] u_{\ell, \ell_0}(r; R) = 2 \sum_{\ell'} [V_{\ell, \ell'}(r; R) + \hat{V}_{\ell, \ell'}(r; R)] u_{\ell', \ell_0}(r; R), \quad (1)$$

where the semicolon denotes the parametric status of R , the value of which is fixed in this approximation. The subscript ℓ_0 denotes the entrance channel, and $k_b^2/2 = \epsilon$ is the energy of the projectile in the body frame (in Hartree units). The quantum number ℓ corresponds to the electronic angular momentum of the scattering electron, and Λ to its projection along the internuclear axis. The coupling potential matrix elements are $V_{\ell, \ell'}(r; R)$ for the static plus (local) correlation-polarization potential and $\hat{V}_{\ell, \ell'}(r; R)$ for the nonlocal exchange operator. We suppress the dependence of all matrix elements, radial functions, and scattering quantities on Λ and on the parity of the system, it being understood that all fixed-nuclei quantities are referred to particular values of these quantum numbers.

The fixed-nuclei R matrix for a particular electron-molecule symmetry, internuclear separation R , and electronic continuum energy ϵ , is defined by [24,25]

$$u_{\ell, \ell_0}(r_0; R) = \sum_{\ell'} R_{\ell, \ell'}(\epsilon; R, r_0) \left[\frac{d}{dr} u_{\ell', \ell_0}(r; R) \right]_{r=r_0}. \quad (2)$$

The sum over ℓ' includes values consistent with the electron-molecule symmetry under consideration (e.g., for the Σ_u symmetry, $\ell' = 1, 3, \dots$). In the EMAP method fixed-nuclei matrices become operators in the nuclear coordinates [18]. Matrix elements of these operators are then evaluated between vibrational wave functions. In order to avoid integrating over poles, the fixed-nuclei R matrix is replaced by the *dimensionless* fixed-nuclei phase matrix defined by the matrix relation

$$\tan \Phi(\epsilon; R, r_0) = \mathbf{k}_b^{1/2} \mathbf{R}(\epsilon; R, r_0) \mathbf{k}_b^{1/2}, \quad (3)$$

where \mathbf{k}_b is a diagonal matrix of (body-frame) wave numbers $k_b = \sqrt{2\epsilon}$. This definition differs from that given previously [17] by the energy-dependent factors of $\mathbf{k}_b^{1/2}$, which render Φ dimensionless.

In conventional scattering theory for a spherical interaction potential, phase shifts are defined relative to free waves via the usual asymptotic boundary conditions [26]. In conventional electron-molecule scattering theory, where the interaction potential is nonspherical, the analogous quantity is the eigenphase sum, which is calculated from the asymptotic K matrix (see Ref. [27], and references therein). The fixed-nuclei phase matrix $\Phi(\epsilon; R, r_0)$, however, is absolute in that it contains the variation with R and ϵ due to the free-electron phase matrix. Relation (2) indicates that, for a free electron, the R matrix is diagonal with elements proportional to the inverse logarithmic derivative of Ricatti-Bessel functions with argument ℓ ,

$$R_{\ell, \ell'}^{\text{FE}}(\epsilon; r_0) = \frac{j_{\ell'}(k_b r_0)}{j_{\ell'}(k_b r_0)} \delta_{\ell, \ell'}. \quad (4)$$

As a consequence of definition (3), the free-electron phase matrix is a diagonal matrix whose elements are proportional to the inverse tangent of the inverse logarithmic derivative of Ricatti-Bessel functions with argument ℓ ,

$$\Phi_{\ell, \ell'}^{\text{FE}}(\epsilon; r_0) \equiv \tan^{-1} \left[\frac{\sqrt{2\epsilon} j_{\ell'}(k_b r_0)}{j_{\ell'}(k_b r_0)} \right] \delta_{\ell, \ell'}. \quad (5)$$

To facilitate resonance analysis for e -H₂ scattering, it is useful to subtract the contribution of the free-electron phase matrix from the fixed-nuclei phase matrix. This subtraction defines the *modified* phase matrix (denoted by the tilde)

$$\tilde{\Phi}(\epsilon; R, r_0) \equiv \Phi(\epsilon; R, r_0) - \Phi^{\text{FE}}(\epsilon; r_0). \quad (6)$$

Were the R matrix radius r_0 extended to infinity, the modified fixed-nuclei phase matrix $\tilde{\Phi}(\epsilon; R, r_0)$ would correspond to the usual eigenphase matrix obtained from the asymptotic reactance matrix \mathbf{K} . For finite r_0 , however, the modified phase matrix incorporates the effects of electron-molecule interactions in the inner region only.

Fixed-nuclei resonances correspond to local maxima of the energy derivative of the eigenphase sum [28,29]. By applying resonance analysis to the modified phase matrix (6), which corresponds to the R matrix radius r_0 , we can define the energy and width of a ‘‘precursor resonance’’ at each internuclear separation [17]. Each fixed-nuclei precursor resonance can be associated with a physical scattering resonance (if one exists) when the R -matrix radius r_0 is extended to infinity. Applying a single-pole Breit-Wigner resonance analysis to the modified fixed-nuclei phase matrix $\tilde{\Phi}(\epsilon; R, r_0)$ at $\epsilon_{\text{res}}(R, r_0)$, we can determine the resonant channel eigenvector $\mathbf{y}(R, r_0)$ and width $\gamma(R, r_0)$ from the eigenvalue equation [30]

$$\frac{d}{d\epsilon} \tilde{\Phi}(\epsilon; R, r_0) \Big|_{\epsilon = \epsilon_{\text{res}}} \mathbf{y}(R, r_0) = \frac{2}{\gamma(R, r_0)} \mathbf{y}(R, r_0). \quad (7)$$

This precursor resonance analysis can be used to decompose the phase matrix $\tilde{\Phi}(\epsilon; R, r_0)$ into a rapidly varying part, the foreground phase matrix $\tilde{\Phi}^1(\epsilon; R, r_0)$, and a slowly varying background part. The foreground phase matrix then assumes the form

$$\tilde{\Phi}^1(\epsilon; R, r_0) = \mathbf{y}(R, r_0) \tan^{-1} \left[\frac{\gamma(R, r_0)}{2[\epsilon_{\text{res}}(R, r_0) - \epsilon]} \right] \mathbf{y}^\dagger(R, r_0). \quad (8)$$

The background phase matrix is defined by subtraction as

$$\tilde{\Phi}^0(\epsilon; R, r_0) \equiv \tilde{\Phi}(\epsilon; R, r_0) - \tilde{\Phi}^1(\epsilon; R, r_0). \quad (9)$$

The method presented here prescribes, for both the background and foreground phase matrices, the formal replacement of the fixed-nuclei electronic energy ϵ by the operator [21]

$$\hat{\epsilon} \equiv E - \hat{\mathcal{H}}^{(v)}, \quad (10)$$

where $\hat{\mathcal{H}}^{(v)}$ is the vibrational Hamiltonian. This operator acts on functions of the vibrational coordinates. The foreground vibronic phase matrix is therefore constructed using a complete set of eigenfunctions $\chi_s(R)$ obtained by solving the eigenvalue equation

$$[\hat{\mathcal{H}}^{(v)} + \epsilon_{\text{res}}(R, r_0)] \chi_s(R) = E_s \chi_s(R) \quad (11)$$

at r_0 in a basis of spline-delta functions [31]. [For clarity, we suppress the dependence of $\chi_s(R)$ and E_s on the R -matrix radius r_0 .] The (v, v') block of the vibronic foreground phase matrix is then calculated from

$$\begin{aligned} \tilde{\Phi}_{v, v'}^1(E; r_0) &= \tan^{-1} \sum_s \langle \phi_v | \mathbf{y}(R, r_0) \gamma^{1/2}(R, r_0) | \chi_s \rangle \\ &\times \frac{1}{2(E_s - E)} \langle \chi_s | \gamma^{1/2}(R, r_0) \mathbf{y}^\dagger(R, r_0) | \phi_{v'} \rangle. \end{aligned} \quad (12)$$

The separation of $\gamma(R, r_0)$ into the product $\gamma^{1/2}(R, r_0) \gamma^{1/2}(R, r_0)$ is essential for the extension of this method to dissociative attachment, and has been discussed in Ref. [17].

The vibronic background phase matrix is obtained using the EMAP method, according to which the matrix elements are

$$\tilde{\Phi}_{v, v'}^0(E) = \langle \phi_v | \tilde{\Phi}_{v, v'}^0(\epsilon; R, r_0) | \phi_{v'} \rangle. \quad (13)$$

Because threshold behavior has been already introduced in the modified phase matrix (6), it is appropriate here to choose the continuum energy ϵ as the geometric mean [21]

$$\epsilon_{v, v'} \equiv [(E - E_v)(E - E_{v'})]^{1/2}. \quad (14)$$

Finally, the (v, v') submatrices of the resulting vibronic R matrix are calculated from the matrix relation

$$\begin{aligned} \mathbf{R}_{v, v'}(E) &= \mathbf{k}_v^{-1/2} \tan[\tilde{\Phi}_{v, v'}^0(E) + \tilde{\Phi}_{v, v'}^1(E) \\ &+ \Phi^{\text{FE}}(E) \delta_{v, v'}] \mathbf{k}_{v'}^{-1/2}. \end{aligned} \quad (15)$$

Note that, in this equation, the free-electron phase matrix, which is independent of the internuclear separation, has been reintroduced. The energy-dependent factors $(k_v k_{v'})^{-1/2}$ in each (v, v') submatrix result from the definition of the dimensionless fixed-nuclei phase matrix. It is important to note that in this analysis the threshold behavior of the scattering matrices arises from the free-electron phase matrix. The unmodified R matrix, used in previous versions of the EMAP and NADP methods, does not contain information relevant to physical boundary conditions outside the R -matrix radius r_0 . Similarly, in the vibronic R matrix given by Eq. (15), branch-point behavior above each vibronic channel threshold is canceled by these energy-dependent factors. Analytic continuation into closed channels below threshold should remove the apparent branch points.

III. IMPLEMENTATION

The coupling potentials in the integrodifferential equations (1) contain static, exchange, and correlation-polarization terms. We calculate each component of the e - H_2 interaction potential from near-Hartree-Fock electronic ground-state target wave functions on a grid of internuclear separations R determined by the probability density of the ground vibrational state. To obtain these electronic functions, we solve the electronic Schrödinger equation of the molecule variationally [32] using a symmetry-adapted basis of contracted nucleus-centered Gaussian type orbitals. This basis includes compact polarization functions that allow for bond formation [33] in the neutral molecule. When used to determine the polarization potential described below, this basis is augmented by additional diffuse functions to allow for distortion of the neutral by the scattering electron. We use a $(5s2p/3s2p)$ basis for the neutral and a $(6s3p/4s3p)$ basis for the polarized molecule. The exponents and contraction coefficients for these bases appear in Table I of Ref. [34]. The quadrupole moment produced by the resulting static potential, averaged over the ground-state vibrational (Morse) wave function of the target, is $0.4772ea_0^2$, as compared to the experimental value [35,36] of $(0.4704 \pm 0.034)ea_0^2$. We treat the exchange potential rigorously as a nonlocal operator [37,38], using in the exchange kernel the same (unaugmented) near-Hartree-Fock molecular orbitals as were used to calculate the static potential (for details, see Ref. [27]).

The final component of our interaction potential accounts for (long-range) polarization and (short-range) correlation and dynamic distortion effects with a local, energy-independent potential. This function includes all *adiabatic* polarization effects exactly via linear variational calculations on the polarized and unpolarized target (Refs. [34,39] detail the calculation of these potentials for e - H_2). This potential further allows for nonadiabatic (correlation) effects via a non-penetrating approximation [40] according to which the two-electron bound-free electrostatic interactions are set to zero whenever the radial coordinate of the projectile is less than that of the one-particle density function of the target. For e - H_2 , this potential can be very accurately represented

by the *dipole* term in the moment expansion of this potential [39]; hence we have adopted the form christened by Gibson and Morrison [34,39] the “better-than-adiabatic dipole” (BTAD) potential. This potential is parameter free. Analytic forms for the equilibrium BTAD potentials for e -H₂ are given in Eqs. (6) and (7) of Ref. [41]. From the asymptotic form of this potential at each R we extract the polarizabilities $\alpha_0(R)$ and $\alpha_2(R)$. The averages of these values over the ground vibrational state are $5.4367a_0^3$ and $1.4575a_0^3$, respectively. These polarizabilities can be assessed by comparison to the experimental values $(5.4263 \pm 0.02)a_0^3$ for the spherical polarizability, as determined from measurements of the refractive index at 290 K [42], and $(1.3567 \pm 0.0023)a_0^3$ for the nonspherical polarizability, as determined in molecular-beam resonance experiments [43].

We calculate the vibrational wave functions in the vibrational close-coupling (VCC) and adiabatic (EMAP, NADP) calculations reported here from the Morse potential

$$V(R) = D_e(e^{-2\alpha x} - 2e^{-\alpha x}), \quad (16)$$

where $x \equiv (R - R_e)/R_e$. For H₂, the dissociation energy at equilibrium is $D_e = 0.1819E_h$, and the parameter α , determined from measured spectroscopic constants [44], is $\alpha = 1.4110$.

Fixed-nuclei R matrices are constructed at a radius $r_0 = 10.0a_0$ for a grid of 45 electronic energies which vary from 0.005 to 10.0 eV. For H₂, this R -matrix radius ensures that the molecular bound-state wave functions have effectively vanished at r_0 , and consequently that exchange is fully included in the inner region. For scattering in the Π_u and Σ_g symmetries, fixed-nuclei R matrices are calculated at internuclear separations $0.5a_0, 0.8a_0, 1.0a_0, 1.2a_0, 1.4a_0, 1.6a_0, 1.8a_0, 2.0a_0, 2.2a_0, 2.4a_0,$ and $2.5a_0$. To account for the rapid variation of the fixed-nuclei phase matrix as a function of internuclear separation in the Σ_u symmetry, additional fixed nuclei R matrices are included for internuclear separations $0.7a_0, 0.9a_0, 1.1a_0, 1.3a_0, 1.5a_0, 1.7a_0, 1.9a_0, 2.1a_0,$ and $2.3a_0$.

At each value of the fixed-nuclei electronic energy and of the internuclear separation, the fixed-nuclei R matrices, multiplied by an appropriate energy factor as in Eq. (3), are diagonalized, and fixed-nuclei phase matrices are constructed from the inverse tangents of the eigenvalues using the corresponding eigenvectors. Multiples of π are added to the resulting eigenvalues in order to ensure a smooth variation with both energy and internuclear separation. If the fixed-nuclei R matrices have degenerate eigenvalues at particular values of electronic energy and internuclear separation, then additional multiples of π are added over the whole energy range and for all internuclear separations, in order to ensure a smooth variation of the phase matrix in regions where R -matrix eigenvalues exhibit avoided crossings. Far from such regions, the matrix of eigenvectors is close to a unit matrix. In this situation, multiples of π can be added independently to each of the eigenvalues, i.e., to the fixed-nuclei phase matrix. In contrast, when the eigenvalues of the fixed-nuclei R matrix exhibit avoided crossings, the corresponding matrix of eigenvectors deviates significantly from a unit matrix. In such situations, the independent addition of multiples

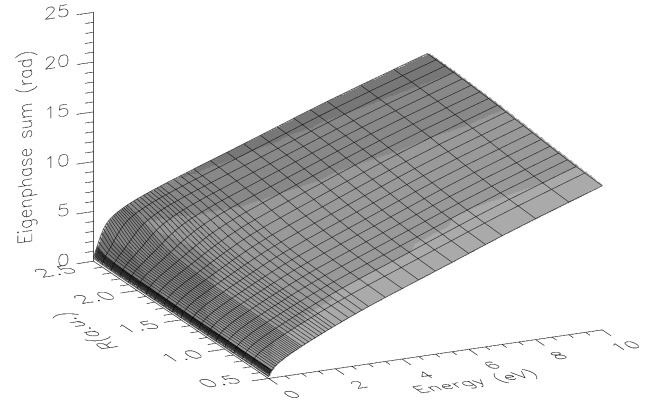


FIG. 1. The precursor eigenphase sum for e -H₂ scattering in the Σ_u symmetry evaluated from fixed-nuclei phase matrices at $r_0 = 10a_0$.

of π to each inverse tangent of the eigenvalues results in adding nonintegral multiples of π to the phase matrix.

Outside the R -matrix region ($r > r_0$), powerful computational methods facilitate solving the scattering equations out to a matching radius in the asymptotic region where the scattering matrix can be extracted. In this outer region, we explicitly allow for vibrational coupling, including vibrational states in the coupled equations for $v \leq 3$. Here the interaction potential is local, a combination of terms due to permanent multipole moments of the target (predominantly the quadrupole interaction) and terms due to polarization distortions of the target induced by the projectile, which in this region can be considered to move adiabatically with respect to these distortions [45]. For low-energy e -H₂ scattering, one need include only the induced polarizability interaction [34]. The vibronic R matrix [Eq. (15)] at $r_1 = 100a_0$ is calculated from its counterpart at the boundary of the R -matrix region r_0 using standard R -matrix propagation methods [46–49]. For large enough radial values ($r > r_1 > r_0$), these adiabatic polarization potentials reduce to their analytic multipolar forms [39]. In this outermost region, beyond r_1 , the coupled scattering equations can be solved by asymptotic expansions, which are evaluated analytically by converting the (divergent) asymptotic series to continued fractions [50–52].

To complete the description of the scattering matrix, we require elements for symmetries other than the lowest three ($\Sigma_g, \Sigma_u,$ and Π_u), and for partial waves within these three symmetries of order higher than are required to converge the fixed-nuclei R matrix at r_0 . (In the present fixed-nuclei calculations for $r \leq r_0$ we include four partial waves per symmetry.) We calculate these additional K -matrix elements using the first Born approximation which, because of the centrifugal barrier term in the effective Hamiltonian for the scattering electron, gives accurate approximations to K -matrix elements at any scattering energy for sufficiently high ℓ (for further discussion, see Refs. [53] and [54]).

Figure 1 shows the variation in the Σ_u symmetry of the precursor eigenphase sum as a function of the fixed-nuclei electronic energy ϵ and internuclear separation R . We emphasize that this quantity is not the physical eigenphase sum one would calculate from the asymptotic K matrix [28]; rather it is the analogous quantity calculated from the fixed-nuclei phase matrix at the R -matrix boundary $r_0 = 10a_0$. This

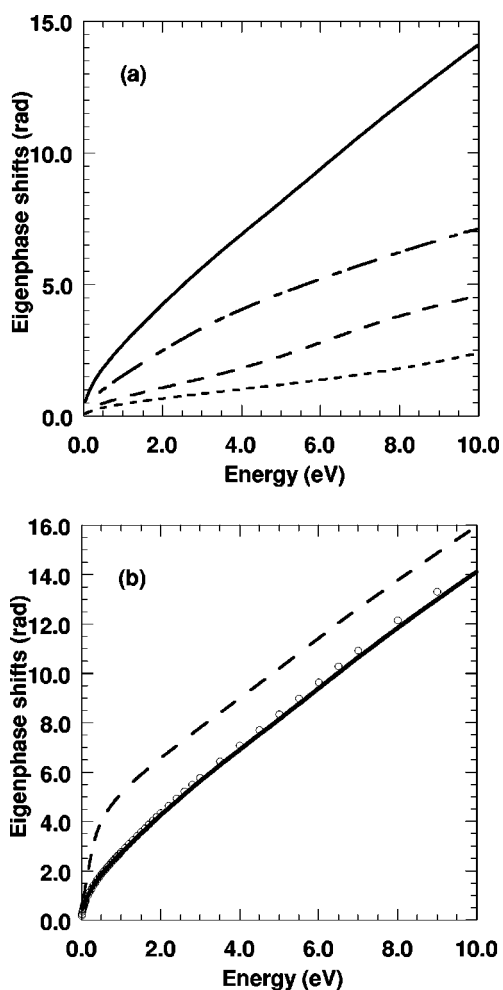


FIG. 2. (a) Free-electron eigenphase shifts and their sum (solid line) for the dominant partial waves of scattering in the Σ_u symmetry, $l=1, 3$, and 5 . (b) Fixed-nuclei Σ_u precursor eigenphase sums at the extreme values of internuclear separation that are relevant to the $0 \rightarrow 1$ and $0 \rightarrow 2$ excitations, $R=0.5a_0$ and $R=2.5a_0$. Also shown is the sum of the free-electron eigenphases (open circles) from (a) (solid line).

quantity is a smooth function of both ϵ and R . For each value of the internuclear separation, the Σ_u eigenphase sum increases rapidly with increasing energy. This behavior is especially pronounced at large values of R , where the precursor eigenphase sum shows a rapid variation for energies from threshold to around 1.0 eV. This characteristic behavior of the eigenphase sum above threshold and at internuclear separations near $2.5a_0$ corresponds to a true fixed-nuclei resonance when r_0 is extended into the asymptotic region.

As the internuclear separation decreases, however, this precursor resonance structure vanishes for values of internuclear separation less than $2.0a_0$; there the precursor eigenphase sum tends to a smooth function of the energy. To understand the behavior of this quantity better, it is useful to consider its counterpart for a free electron.

In Fig. 2(a), we show the variation of diagonal elements of the free-electron phase matrix calculated at $r=10a_0$ for partial wave orders $l=1, 3$, and 5 , the dominant contributions to the Σ_u precursor eigenphase sum. As expected from Eq. (5), the diagonal elements of the phase matrix are non-

linear functions of the energy ϵ that exhibit characteristic behavior near threshold due to the energy-dependent factor $k=\sqrt{2\epsilon}$. In Fig. 2(b), we compare the Σ_u eigenphase sum for our smallest and largest values of R , $0.5a_0$ and $2.5a_0$, to the sum of the diagonal elements of the free-electron phase matrix to the Σ_u symmetry. This comparison indicates that the variation of the precursor eigenphase sum is largely determined by that of the corresponding free-electron eigenphase sum. By considering the difference between these two quantities, we see that, like the asymptotic eigenphase sum, the precursor eigenphase sum of Fig. 2 shows a pronounced resonance structure near threshold for large values of R . By contrast, for small values of R the precursor resonance is superimposed on a strongly decreasing background and is difficult to characterize.

This point is reinforced in Fig. 3(a), which shows the variation of the *modified* phase matrix (the fixed-nuclei phase matrix minus the free-electron matrix) as a function of ϵ and R . This variation closely resembles that of the asymptotic eigenphase sums calculated from the Σ_u K matrix [13]. It is important to recall that the quantity shown in Fig. 3(a) depends on the R -matrix radius, and as such only includes the effect of the potential in the inner region, $r \leq r_0$. Figures 3(b) and 3(c), respectively, show the variation with R and ϵ of the background and foreground phase matrices obtained when the precursor resonance analysis described in Sec. II is applied to the modified phase matrix. These graphs demonstrate that this analysis leads to a background phase matrix which varies smoothly with R and ϵ , while the rapidly varying part of the modified phase matrix is described by the foreground phase matrix. This point further illustrates the reason for using two different methods—the EMAP and NADP approximations—to treat vibrational dynamics in the background and foreground phase matrices, respectively.

The variation with internuclear separation of the precursor resonance energy curve and the corresponding width obtained by the resonance analysis are shown in Figs. 4(a) and 4(b). Figure 4(a) shows that the precursor resonance energy curve differs from the potential of the target molecule for all internuclear separations. The corresponding width in Fig. 4(b) increases rapidly with decreasing R , and the resonance fades smoothly into the background and ceases to affect the vibrational dynamics significantly. *Yet at these small values of the internuclear separation the decomposition of the phase matrix continues to be well defined, even though its physical effects are negligible.* Electron scattering from H_2 is prototypical of situations in which a fixed-nuclei resonance has a minimal influence on excitation to the first vibrational state. A comparison between $v_0=0$ to $v=1$ cross sections from NADP and EMAP calculations in the Σ_u symmetry is therefore particularly useful as a test of this assumption and will be the subject of the next section.

Finally, we emphasize that the computational implementation of relation (12) requires special care due to avoided crossing in the eigenvalues of the vibronic foreground R matrix. It should be noted that this inconvenience depends on the system as well as on assumptions inherent in the interaction potential. It arises in the present application because of the large range of energies under consideration, from 0 to 10.0 eV. To overcome this difficulty, irregularities in the foreground vibronic phase matrix (12) are identified by comparison to the equivalent transformation

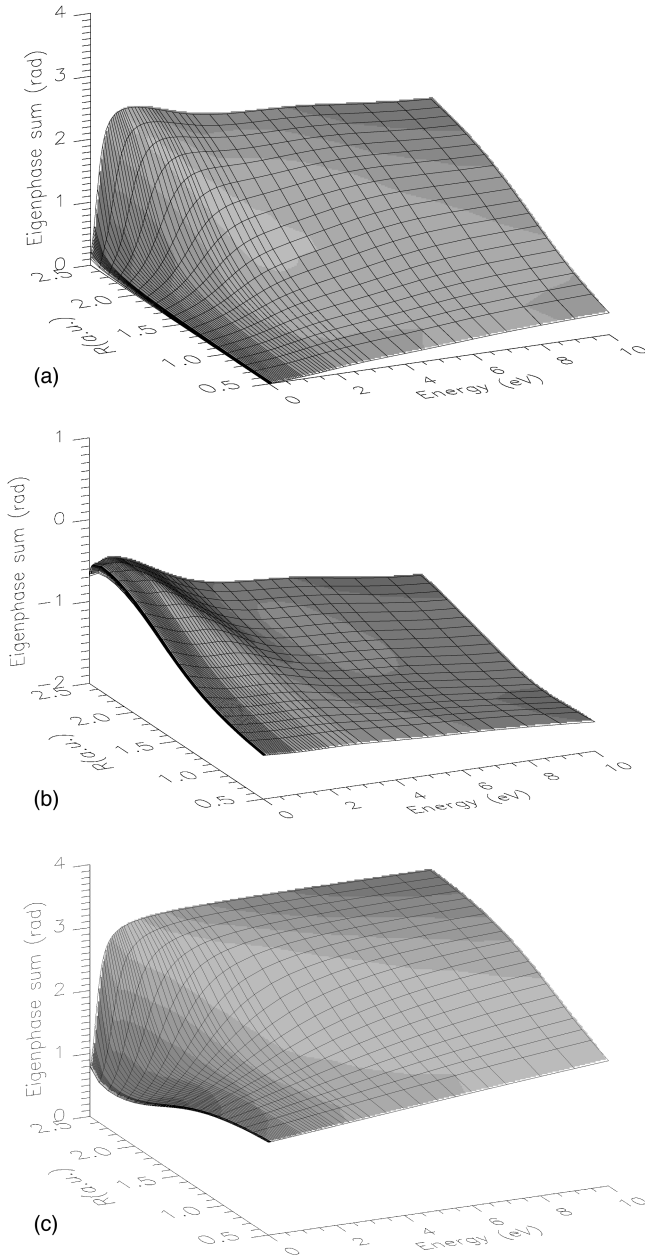


FIG. 3. (a) Modified precursor eigenphase sums for e -H₂ scattering in the Σ_u symmetry, evaluated from fixed-nuclei phase matrices at $r_0=10a_0$ by subtracting the free-electron phase matrix from the fixed-nuclei precursor eigenphase matrix. This phase matrix is decomposed into (b) background and (c) foreground parts, as described in the text.

$$\begin{aligned} \tilde{\Phi}_{v,v'}^1(E) = & \sum_{s,s'} \tan^{-1} \langle \phi_v | \mathbf{y}(R, r_0) | \chi_s \rangle \\ & \times \langle \chi_s | \left[\frac{\gamma(R, r_0)}{(E_s - E) + (E_{s'} - E)} \right] | \chi_{s'} \rangle \\ & \times \langle \chi_{s'} | \mathbf{y}^\dagger(R, r_0) | \phi_{v'} \rangle. \end{aligned} \quad (17)$$

When found, irregular elements of the phase matrix are replaced by values from this relation. Equation (17) is obtained by twice introducing the complete set of eigenfunctions

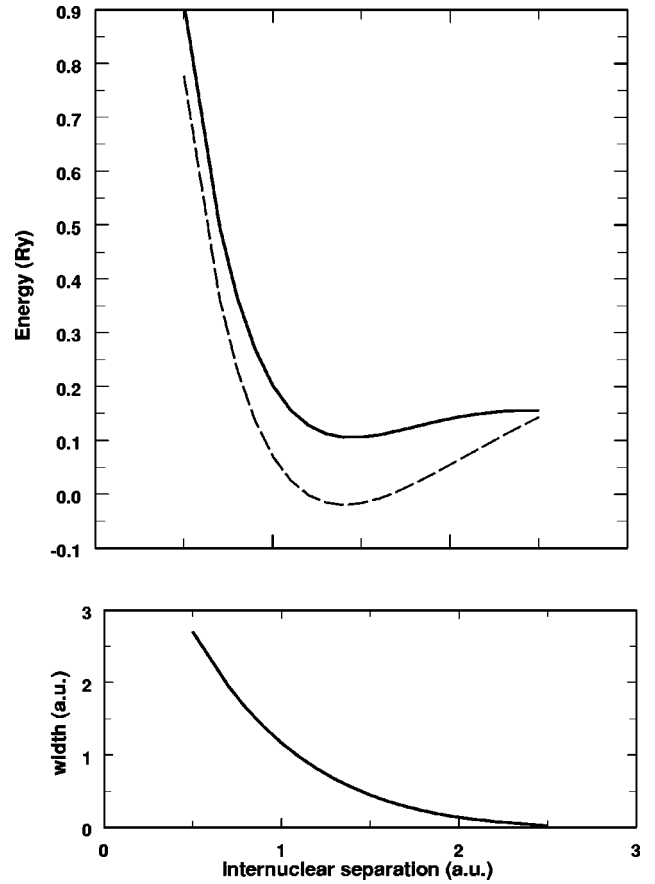


FIG. 4. (a) The effective potential energy for the precursor resonance (solid line): the sum of $\epsilon_{\text{res}}(R, r_0)$ and the ground electronic state potential energy of H₂, represented by a Morse potential (long dashed line) (b). Variation of the precursor resonance width function $\gamma(R, r_0)$ with internuclear separation. Both quantities were calculated at the R -matrix radius $r_0=10a_0$.

$\{\chi_s(R)\}$ in Eq. (8), and by choosing as the continuum energy the *arithmetic* mean of the eigenvalues of the operator $\epsilon_{\text{res}} - \hat{\epsilon}$. Despite this approximation, Eq. (17) allows a direct construction of the vibronic phase matrix without the need to diagonalize the corresponding R matrix. Where valid, this alternative procedure thus allows a construction of the vibronic foreground phase matrix even if the vibronic resonant R -matrix eigenvalues manifest avoided crossings.

IV. RESULTS

In this section we investigate the validity of the phase matrix decomposition (9) and of the NADP method via a systematic comparison of NADP integral and differential cross sections against results from its fully adiabatic counterpart, the EMAP method, and from fully nonadiabatic VCC calculations. We consider excitations to the $v=1$ and 2 states. The thresholds for these states are 0.5156 and 1.001 127 eV, respectively [44].

A. Integral cross sections

Partial integral cross sections in the dominant e -H₂ symmetries (Σ_g , Σ_u , and Π_u) and their sum, as calculated using the NADP, EMAP, and VCC methods are shown in Fig. 5

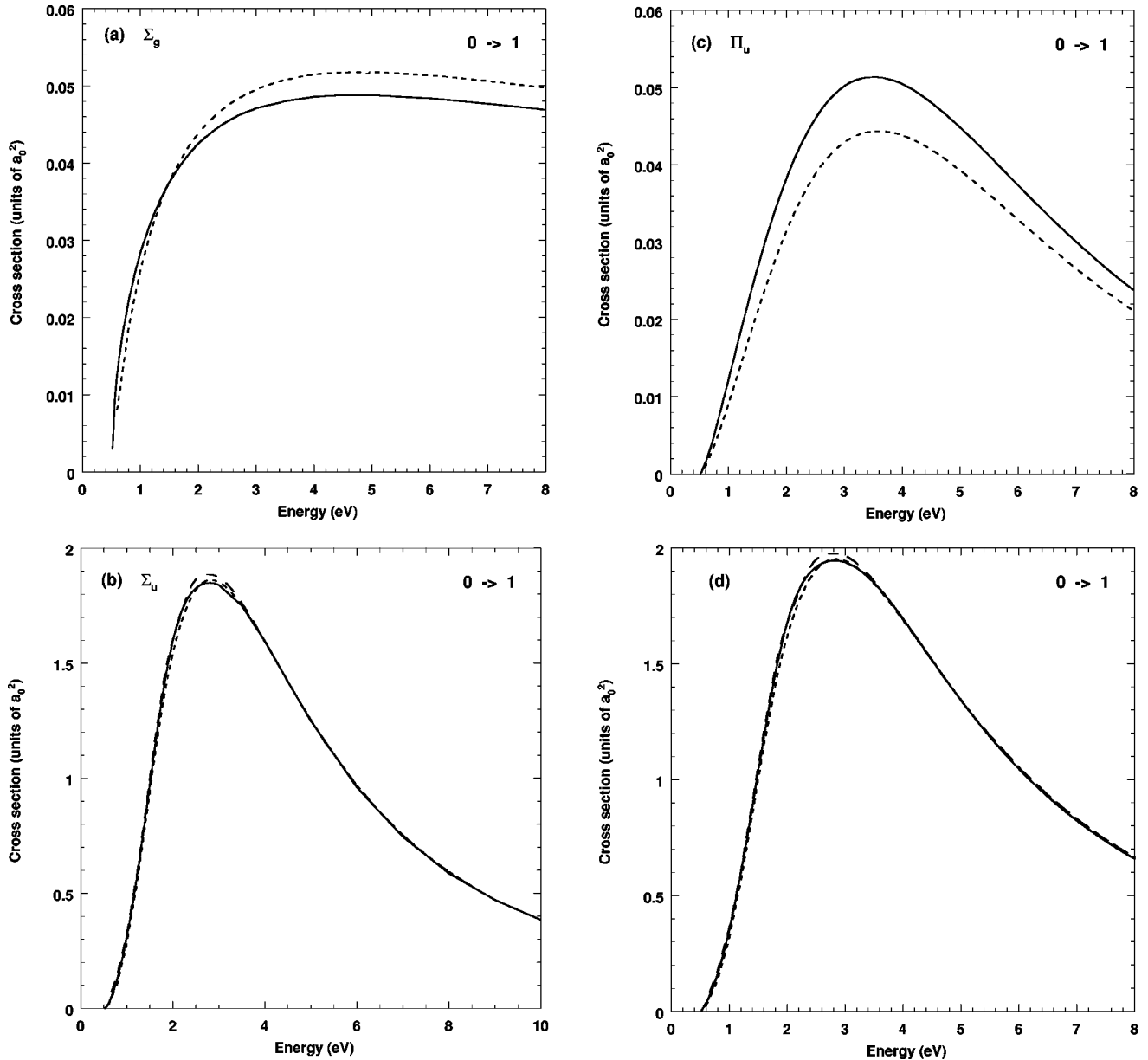
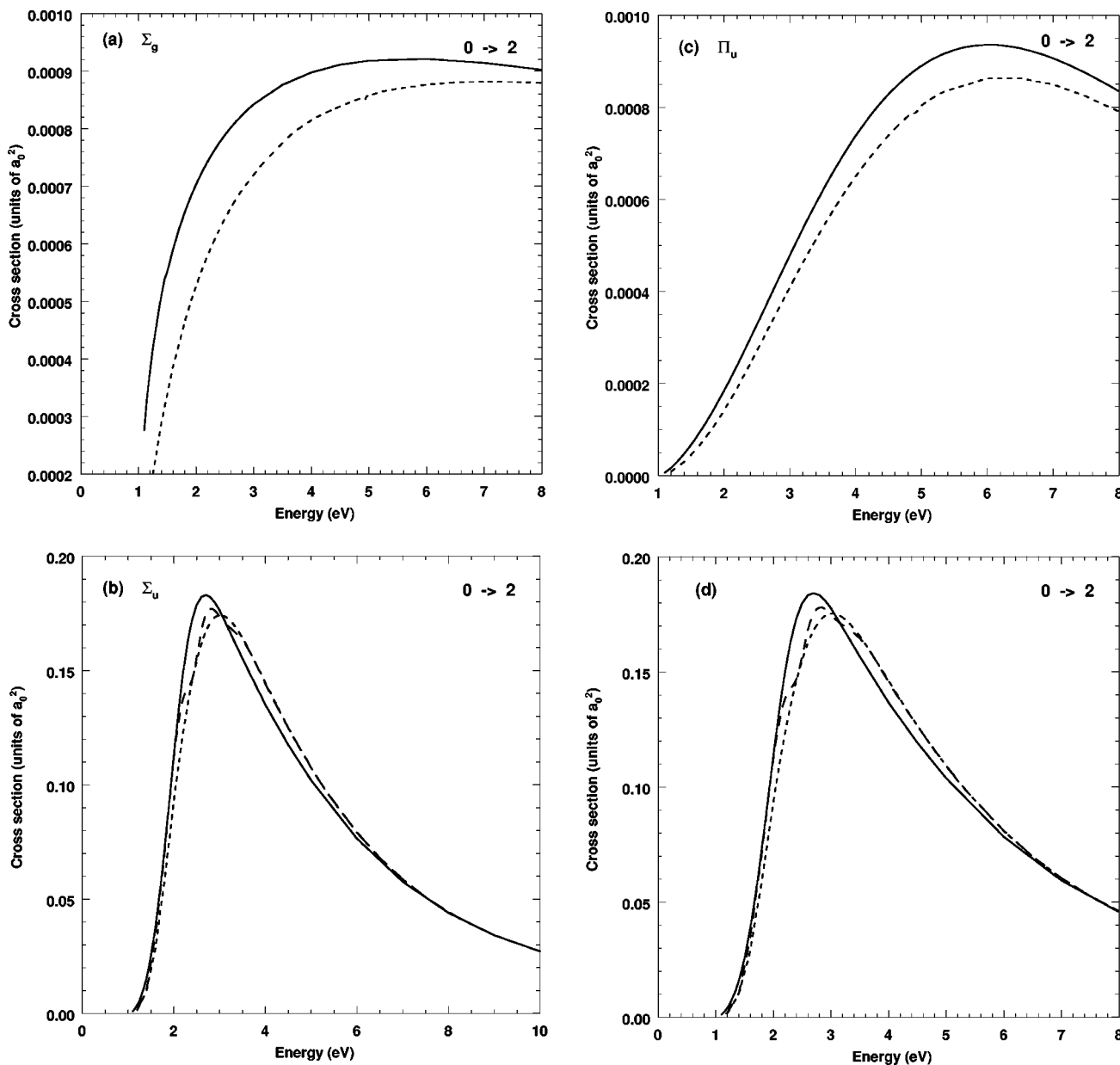


FIG. 5. Partial integral cross sections in the (a) Σ_g , (b) Σ_u , and (c) Π_u symmetries for the $0 \rightarrow 1$ vibrational excitation of H_2 and (d) their sum. Results for the EMAP (short dashed line) and NADP (long dashed line) approximations are compared with benchmark VCC results (solid line).

for $v=1$ and in Fig. 6 for $v=2$. These data are presented at selected energies in Table I; a full list is available from the authors upon request. Comparison between the NADP and EMAP cross sections in Figs. 5 and 6 validates the decomposition of the fixed-nuclei phase matrix into foreground and background parts even for small values of the internuclear separation, where no physical resonance appears in the (asymptotic) fixed-nuclei eigenphase sum. Furthermore, comparison to the VCC results shows that both the EMAP and NADP methods provide a reliable description of e - H_2 partial cross sections even in the acutely sensitive energy regime near threshold. Cross sections in this energy region are especially sensitive to conservation of energy in the collision; violation of this requirement is the reason for the failure near threshold of the usual adiabatic-nuclear-vibration approximation [2,55,56].

The EMAP approximation does not account rigorously for the loss of kinetic energy of the continuum electron during excitation; this energy loss is properly included in adiabatic theories that use off-shell fixed-nuclei scattering matrices, such as the first-order nondegenerate adiabatic approximation [9,10]. However, the EMAP method improves on the conventional adiabatic-nuclei approximation by calculating elements of the vibronic phase matrix at energies appropriate to each vibrational channel. In the present implementation, the geometric mean (14) of the eigenvalues of the operator $\hat{\epsilon}$ are used, so precise agreement of the EMAP and VCC results is not expected. It should be noted, however, that here, as in applications of the EMAP method directly to the asymptotic K matrix [13], this procedure does provide a reliable description of the inelastic cross section without imposing the computational burden of off-shell

FIG. 6. Same as 5 for the $0 \rightarrow 2$ excitation.

fixed-nuclei scattering calculations. For both excitations, VCC, NADP, and EMAP cross sections tend to the same values for scattering energies large enough that the loss of kinetic energy of the continuum electron is negligible compared to the scattering energy, i.e., above about 7.0 eV.

For the $0 \rightarrow 1$ cross section in Fig. 5, comparison of VCC and NADP results confirms the ability of the NADP to incorporate nonadiabatic effects for this excitation. The comparison between EMAP and VCC results for this excitation shows that nonadiabatic effects exert minimal influence on this cross section at energies near the enhancement at 3.0 eV.

More interesting is the corresponding comparison of the $0 \rightarrow 2$ cross sections in Fig. 6. For this excitation larger differences are evident between NADP, EMAP, and VCC results, especially in the magnitude and position of the maximum in the Σ_u and total cross sections. These differences clearly indicate that the fixed-nuclei resonance at large inter-

nuclear separations influences the $0 \rightarrow 2$ cross section more than the $0 \rightarrow 1$ cross section—hence the need to account for nonadiabatic effects to describe the former process accurately.

Although the maximum value of the $0 \rightarrow 2$ NADP cross section appears in good agreement with its VCC counterpart, a mild dip is evident in the NADP result at energies between 2.0 and 3.0 eV. Within the limits of the interaction potential used to calculate the fixed-nuclei R matrices, which is based on a Hartree-Fock representation of the electronic ground state wave function, the NADP method appears to overestimate the influence of the nonadiabatic effects slightly in this energy region.

The accuracy of these results is limited by the discrete set of internuclear separations used in the calculations. For NADP and VCC calculations, the largest values of internuclear separation are $2.5a_0$ and $2.6a_0$, respectively. Further-

TABLE I. Partial integral cross sections (in a_0^2) and their sum (the total $0 \rightarrow 1$ cross section) for e - H_2 scattering at selected energies from the following theories: vibrational close coupling (VCC: top line for each energy), the nonadiabatic phase matrix (NADP) method (second line), and the energy-modified adiabatic phase matrix (EMAP) approximation (third line). The NADP method is required only for the Σ_u symmetry; the ‘‘NADP total cross sections’’ in the last column therefore include EMAP contributions from the Σ_g and Π_u symmetries.

E	Method	Σ_g	Σ_u	Π_u	total
0.60	VCC	0.0126	0.0211	0.0013	0.0349
	NADP	—	0.0316	—	0.0405
	EMAP	0.0081	0.0149	0.0008	0.0238
0.80	VCC	0.0222	0.1331	0.0063	0.1616
	NADP	—	0.1522	—	0.1754
	EMAP	0.0187	0.1124	0.0045	0.1356
1.20	VCC	0.0327	0.5449	0.0181	0.5957
	NADP	—	0.5578	—	0.6033
	EMAP	0.0316	0.5152	0.0138	0.5607
1.40	VCC	0.0361	0.8241	0.0239	0.8841
	NADP	—	0.8451	—	0.8996
	EMAP	0.0359	0.7960	0.0186	0.8505
1.60	VCC	0.0387	1.1187	0.0292	1.1866
	NADP	—	1.1500	—	1.2120
	EMAP	0.0391	1.0860	0.0232	1.1480
2.00	VCC	0.0425	1.5974	0.0382	1.6781
	NADP	—	1.6000	—	1.6750
	EMAP	0.0438	1.5420	0.0314	1.6170
3.00	VCC	0.0471	1.8415	0.0502	1.9388
	NADP	—	1.8740	—	1.9660
	EMAP	0.0495	1.8520	0.0429	1.9440
4.00	VCC	0.0486	1.5967	0.0505	1.6957
	NADP	—	1.5980	—	1.6930
	EMAP	0.0514	1.5950	0.0439	1.6900
5.00	VCC	0.0488	1.2505	0.0449	1.3442
	NADP	—	1.2530	—	0.1344
	EMAP	0.0518	1.2550	0.0393	1.3460
7.00	VCC	0.0477	0.7464	0.0301	0.8242
	NADP	—	0.7532	—	0.8304
	EMAP	0.0506	0.7541	0.0266	0.8313
8.00	VCC	0.0469	0.5885	0.0238	0.6592
	NADP	—	0.5940	—	0.6648
	EMAP	0.0497	0.5946	0.0211	0.6654

more, the NADP and EMAP methods are based on matrix relations and, for the Σ_u symmetry, require a calculation of vibrational submatrices (v, v') of the phase matrix for vibrational quantum numbers larger than that of the final state of the excitation of interest. Thus, for the $0 \rightarrow 2$ cross sections in Figs. 6, vibronic phase matrices were constructed using blocks for v and v' from 0 to 3. This may introduce a slight error, because, for e - H_2 scattering, the $v = 3$ vibrational state is appreciable at $R = 2.5a_0$. The errors due to renormalization of the vibrational wave function on the interval of internuclear separations considered here, and to neglect of higher values of R where the fixed-nuclei resonance is even more pronounced, are difficult to assess.

B. Differential cross sections

Because differential cross sections (DCS's) are more sensitive to the scattering dynamics than integral cross sections, they more clearly reveal the strengths and weaknesses of the approximations inherent in the NADP and EMAP methods. Figures 7 and 8 show DCS's at selected energies for the $0 \rightarrow 1$ and $0 \rightarrow 2$ excitations. The most significant differences in the $0 \rightarrow 1$ DCS's of Fig. 7 appear at 0.8 eV, an energy near the threshold of this excitation at 0.516 eV. Figure 7(a) shows that at 0.8 eV nonadiabatic effects are somewhat more important for scattering angles $\theta \geq 90^\circ$ than at smaller angles. Throughout the angular range, the NADP method slightly overestimate the DCS's, while the EMAP method underestimates them, most noticeably for $\theta < 90^\circ$. These differences are washed out by integration over scattering angle in the integral cross sections shown in Fig. 5. As the energy increases and nonadiabatic effects become negligible, both methods reproduce the VCC cross sections well. Note that this statement holds even at 3.0 eV, the peak of the broad, weak resonance in this cross section.

More pronounced differences are evident at the lowest energy in Fig. 8, the $0 \rightarrow 2$ DCS's at 1.6 eV. Both approximations underestimate these cross sections, with the NADP result closer to the VCC values at all angles. At a slightly higher energy, 2.0 eV in Fig. 8(b), the NADP approximation proves excellent while the EMAP approximation still gives a result below the VCC cross section. By 3.0 eV, in Fig. 8(c), all three methods give identical DCS's. But the level of agreement at this energy is slightly misleading. As Fig. 8(d) shows, the EMAP and NADP cross sections move slightly above the VCC result except near the (p -wave) maximum at 90° , where all three agree.

With still further increases in energy (not shown), the EMAP and NADP $0 \rightarrow 2$ DCS's rapidly come into agreement with the VCC results, as happens in Fig. 7 for $0 \rightarrow 1$ DCS's at and above 1.6 eV. For both excitations, this concurrence simply reflects the relative unimportance of nonadiabatic effects for these excitations at energies above a few eV, and the increasing validity of the approximate treatment of energy conservation inherent in the NADP and EMAP methods. This concurrence is not surprising in light of the analogous phenomenon in DCS's from conventional adiabatic-nuclear-vibrational calculations at energies well above threshold [56].

At all energies, $0 \rightarrow 2$ DCS's show the influence of p -wave Σ_u scattering in their shapes, which are essentially symmetric about 90° , although minor contributions from other partial waves are evident below 3.0 eV. By contrast, the $0 \rightarrow 1$ DCS's in Fig. 7 exhibit more substantial partial-wave mixing at all energies. Even at 3.0 eV, the energy of the maximum in the $0 \rightarrow 1$ integral cross section, the DCS's reveal that the scattering is not purely p wave, indicating minimal influence of the large- R fixed-nuclei resonance on this cross section, and suggesting that it may be inappropriate to think of it as ‘‘resonant scattering.’’

Because $\phi_2(R)$, the final-state vibrational wave function for the $0 \rightarrow 2$ excitation, is appreciable at larger values of R than is $\phi_1(R)$, the DCS's for the $0 \rightarrow 2$ excitation are more influenced by the p -wave shape resonance in the fixed-nuclei Σ_u S matrix for large R than are those for the $0 \rightarrow 1$ excita-

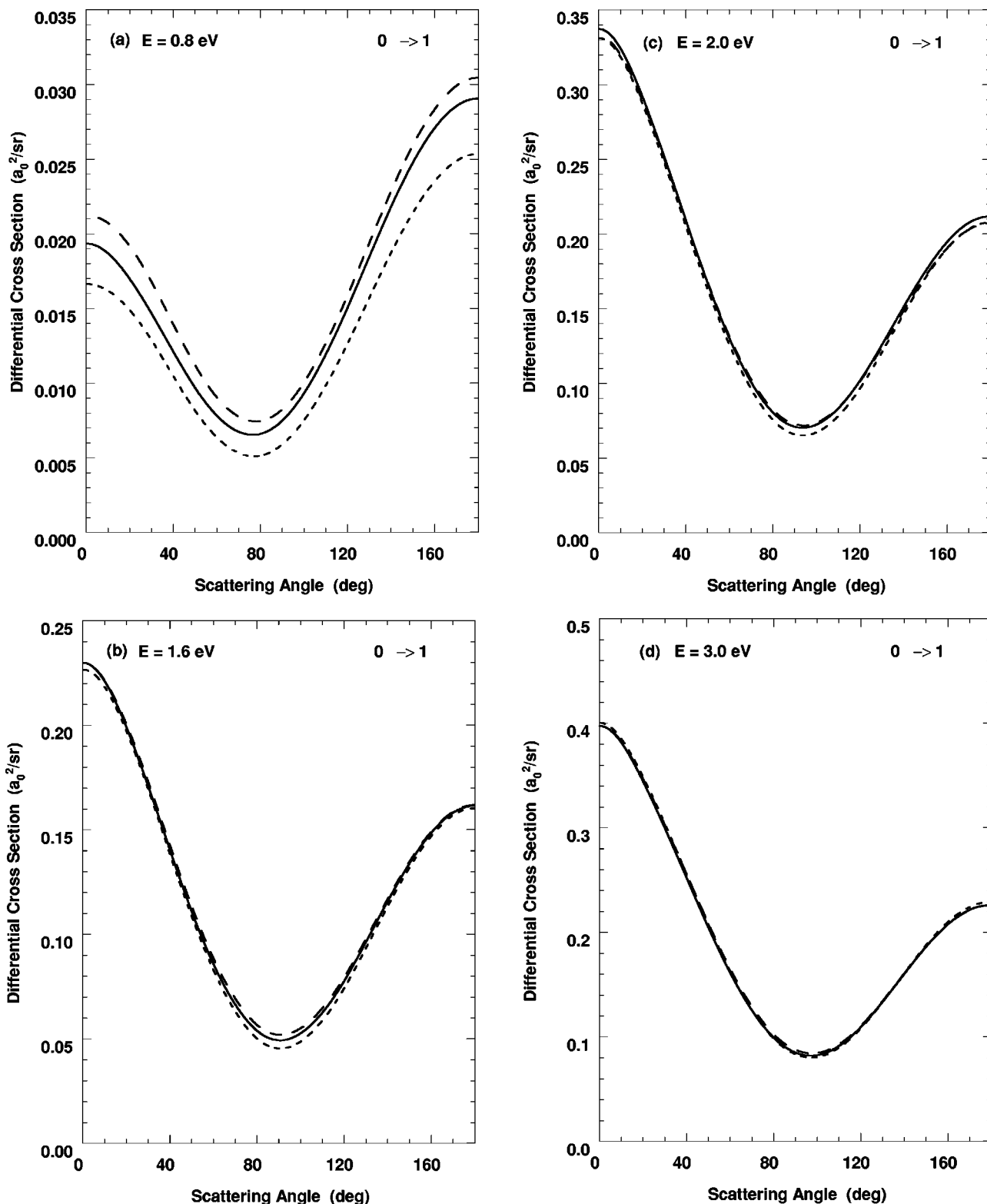


FIG. 7. Differential cross sections for the $0 \rightarrow 1$ vibrational excitation of H_2 at (a) 0.8, (b) 1.6, (c) 2.0, and (d) 3.0 eV. Results for the NADP (long-dashed line) and EMAP (short-dashed line) approximations are compared with benchmark VCC results (solid line).

tion. Consequently, the shape of the $0 \rightarrow 2$ DCS's more clearly manifest the symmetric shape of a p -wave resonance (especially near 3.0 eV) than do the $0 \rightarrow 1$ DCS. This observation is consistent with the increased importance of nonadiabatic effects in this excitation evident in Fig. 6.

Such effects become significantly more important as the final-state vibrational quantum number increases [8]. To il-

lustrate this effect, we conclude with Fig. 9, which shows integral cross sections for the $0 \rightarrow 3$ excitation in H_2 . The NADP cross sections show clear evidence of the characteristic near-resonant structures found when nonadiabatic physics is important [15,14]. This structure is wholly absent from the EMAP cross sections, further verifying their origin in nonadiabaticity.

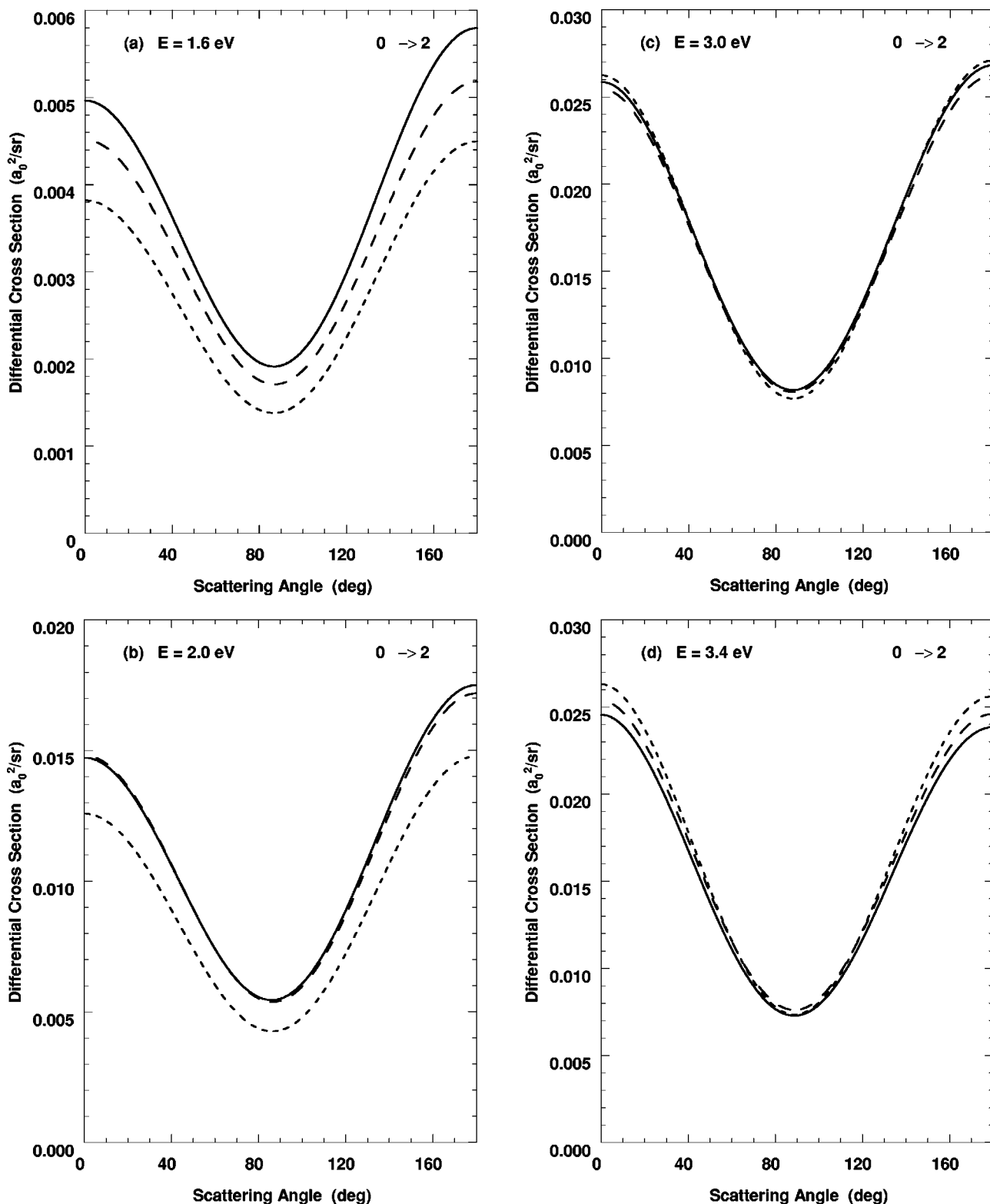


FIG. 8. Differential cross sections for the $0 \rightarrow 2$ vibrational excitation of H_2 at (a) 1.6, (b) 2.0, (c) 3.0, and (d) 3.4 eV. Results for the NADP (long-dashed line) and EMAP (short-dashed line) approximations are compared with benchmark VCC results (solid line).

V. CONCLUSIONS

The NADP method has previously proven its mettle in calculations on resonant $e\text{-N}_2$ scattering [18], where the fixed-nuclei eigenphase sum exhibits an unambiguous shape resonance at all relevant internuclear separations. The pur-

pose of the present paper is to calibrate a modified version of the method which systematically includes nonadiabatic effects for systems in which the range of relevant values of R encompasses quite different scattering mechanisms—here ranging from nonresonant scattering at small R to resonant scattering at large R . The key equations of the present modi-

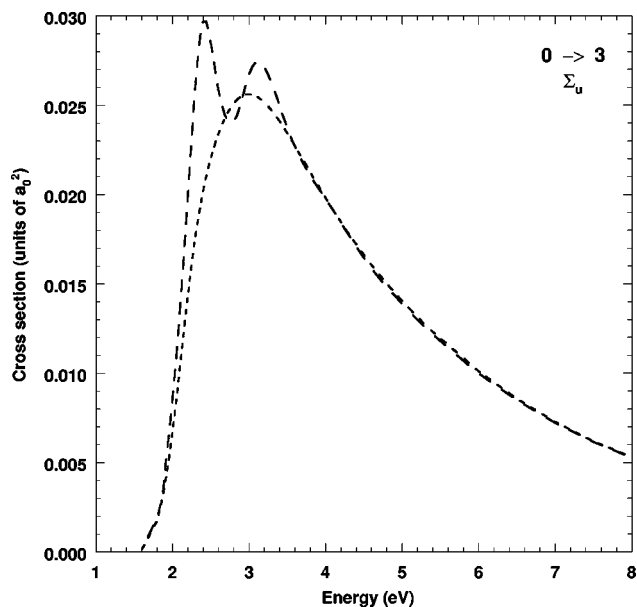


FIG. 9. Partial cross section in the Σ_u symmetry for the $0 \rightarrow 3$ excitation of H_2 as calculated in the NADP (solid curve) and EMAP (dashed curve) approximations.

fied NADP method are the redefinition [Eq. (3)] of the fixed-nuclei phase matrix as dimensionless, and the removal of the free-electron phase matrix (5) prior to the precursor resonance analysis of the foreground phase matrix (8).

The key step in the NADP formalism is the replacement of the fixed-nuclei electronic energy ϵ by the operator $\hat{\epsilon} \equiv E - \hat{\mathcal{H}}^{(v)}$ in the fixed-nuclei foreground phase matrix $\Phi^1(\epsilon; R, r_0)$. This replacement introduces nonadiabatic effects into a procedure that, throughout the inner region $r \leq r_0$, is based solely on fixed-nuclei quantities; it therefore allows a transfer of energy between the kinetic energy of the vibrational motion and the continuum energy of the projectile. In $e\text{-H}_2$ scattering, such an energy transfer is vital to high-lying vibrational excitations ($v_0 = 0 \rightarrow v \geq 3$) and to dissociative attachment.

What enables construction from the resulting operator function $\Phi^1(\hat{\epsilon}; R, r_0)$ of the *vibronic* foreground phase matrix at r_0 is the introduction via closure of the complete set $\{\chi_s(R)\}$ of eigenfunctions of $\hat{\mathcal{H}}^{(v)} + \epsilon_{\text{res}}(R, r_0)$. The effective potential energy for these vibrational eigenfunctions, the sum

of the ground-state electronic energy of H_2 and the fixed-nuclei precursor resonance energy, is the potential curve of Fig. 4, the key computational device of the NADP method. The expansion basis $\{\chi_s(R)\}$ corresponding to this potential therefore represents the effective response of the nuclei to *all* the electrons, bound and continuum, in the system [57].

Two limitations of the NADP method should be kept in mind. First, although the method exploits an R -matrix formalism to connect to formally exact VCC theory outside the R -matrix boundary r_0 , it invokes simplifying approximations inside r_0 . Whereas the VCC method is limited by a necessarily incomplete vibrational basis (which omits the vibrational continuum), the NADP method replaces functions of operators by simplified algebraic forms that neglect certain commutators involving the rovibrational kinetic-energy operator. Thus it is difficult to assess the formal residual errors in a NADP result except by the type of detailed numerical comparisons presented here. Second, the procedure for evaluating off-diagonal matrix elements in the EMAP method, which we use for the background phase matrix, is rather arbitrary, and the resulting formulas may not be appropriate for scattering near threshold, where long-range potentials play an important role. This point requires separate study in particular cases, as has been done for rotational effects in dipolar scattering [18].

The thrust of the comparisons of NADP and VCC integral and differential cross sections for the $0 \rightarrow 1$ and $0 \rightarrow 2$ excitations in Sec. IV are, first, to validate the method by demonstrating concurrence with fully nonadiabatic VCC results, and, second, to probe the breakdown of these approximations elsewhere. Introducing the fully adiabatic EMAP results to this picture reveals, especially in DCS comparisons, the nature and importance of nonadiabatic effects for low-lying vibrational excitations of H_2 . These effects, of course, become far more important for excitation to higher-lying states and for dissociative attachment. It is in the study of such processes, the next stage of this research, that the NADP method as formulated and calibrated here will be most valuable.

ACKNOWLEDGMENTS

We would like to thank Dr. Wayne K. Trail for his assistance with the VCC calculations reported here, Dr. Barry I. Schneider for useful discussions, and the National Science Foundation for support under Grant No. PHY-9722055.

-
- [1] N. F. Lane, *Rev. Mod. Phys.* **52**, 29 (1980).
 [2] M. A. Morrison, *Adv. At. Mol. Phys.* **24**, 51 (1988).
 [3] W. Domcke, *Phys. Rep.* **208**, 97 (1991).
 [4] R. K. Nesbet, *Comments At. Mol. Phys.* **11**, 25 (1981).
 [5] C. W. McCurdy and R. C. Mowrey, *Phys. Rev. A* **25**, 2529 (1982).
 [6] E. DeRose, E. A. Gislason, and N. H. Sabelli, *J. Chem. Phys.* **82**, 4577 (1985).
 [7] T. Gorczyca and D. W. Norcross, *Phys. Rev. A* **42**, 5132 (1990).
 [8] M. Allan, *J. Phys. B* **18**, L451 (1985).
 [9] M. A. Morrison, *J. Phys. B* **19**, L707 (1986).
 [10] M. A. Morrison, M. Abdolsalami, and B. K. Elza, *Phys. Rev. A* **43**, 3440 (1991).
 [11] H. T. Thümmel, T. Grimm-Bosbach, R. K. Nesbet, and S. D. Peyerimhoff, in *Computational Methods for Electron-Molecule Collisions*, edited by W. M. Huo and F. A. Gianturco (Plenum, New York, 1995), Chap. 12, pp. 265–292.
 [12] H. T. Thümmel, R. K. Nesbet, and S. D. Peyerimhoff, *J. Phys. B* **25**, 4533 (1992).
 [13] S. Mazevet, M. A. Morrison, and R. K. Nesbet, *J. Phys. B* **31**, 4437 (1998).

- [14] M. Berman, C. Mündel, and W. Domcke, *Phys. Rev. A* **31**, 641 (1985).
- [15] C. Mündel, M. Berman, and W. Domcke, *Phys. Rev. A* **32**, 181 (1985).
- [16] R. K. Nesbet, in *Collision Processes of Ion, Positron, Electron and Photon Beams with Matter*, Latin American School of Physics, edited by A. C. de Azevedo e Souza *et al.* (World Scientific, New Jersey, 1991), pp. 94–103.
- [17] R. K. Nesbet, *Phys. Rev. A* **54**, 2899 (1996).
- [18] T. Grimm-Bosbach, H. T. Thümmel, R. K. Nesbet, and S. D. Peyerimhoff, *J. Phys. B* **29**, L105 (1996).
- [19] M. L. D. Barry, I. Schneider, and P. G. Burke, *J. Phys. B* **12**, L365 (1979).
- [20] B. I. Schneider, M. L. Dourneuf, and V. K. Lan, *Phys. Rev. Lett.* **43**, 1926 (1979).
- [21] R. K. Nesbet, *Phys. Rev. A* **19**, 551 (1979).
- [22] W. Sun *et al.*, *Phys. Rev. A* **52**, 1229 (1995).
- [23] M. Shugard and A. U. Hazi, *Phys. Rev. A* **12**, 1895 (1975).
- [24] *Atomic and Molecular Processes: An R-Matrix Approach*, edited by P. G. Burke and K. A. Berrington (Institute of Physics, Bristol, 1993).
- [25] B. I. Schneider, in *An R-Matrix Approach to Electron-Molecule Collisions*, edited by W. M. Huo and F. A. Gianturco (Plenum, New York, 1995), Chap. 8, pp. 213–226. See Ref. 58.
- [26] J. R. Taylor, *Scattering Theory* (Wiley, New York, 1972).
- [27] M. A. Morrison and W. Sun, in *Computational Methods for Electron-Molecule Collisions* (Ref. [11]), Chap. 6, pp. 131–190.
- [28] A. Hazi, *Phys. Rev. A* **19**, 920 (1979).
- [29] R. K. Nesbet, *Variational Methods in Electron-Atom Scattering Theory* (Plenum, New York, 1980).
- [30] F. T. Smith, *Phys. Rev.* **118**, 349 (1960).
- [31] R. K. Nesbet and T. Grimm-Bosbach, *J. Phys. B* **26**, L423 (1993).
- [32] J. W. Moskowitz and L. C. Snyder, in *Methods of Electronic Structure Theory*, edited by I. H. F. Schaeffer (Plenum, New York, 1977), p. 387.
- [33] T. Dunning, *J. Chem. Phys.* **55**, 3958 (1971).
- [34] T. L. Gibson and M. A. Morrison, *Phys. Rev. A* **29**, 2479 (1984).
- [35] N. F. Ramsey, *Phys. Rev.* **87**, 1075 (1952).
- [36] A. D. Buckingham, R. L. Disch, and D. A. Dunmur, *J. Am. Chem. Soc.* **90**, 3104 (1968).
- [37] W. K. Trail, M. A. Morrison, W. A. Isaacs, and B. C. Saha, *Phys. Rev. A* **41**, 4868 (1990).
- [38] W. K. Trail, Ph.D. thesis, University of Oklahoma, 1991 (unpublished).
- [39] T. L. Gibson, Ph.D. thesis, University of Oklahoma, 1982 (unpublished).
- [40] A. Temkin, *Phys. Rev.* **107**, 1004 (1957).
- [41] T. L. Gibson and M. A. Morrison, *J. Phys. B* **14**, 727 (1981).
- [42] A. C. Newell and R. C. Baird, *J. Appl. Phys.* **36**, 3751 (1965).
- [43] K. B. MacAdam and N. F. Ramsey, *Phys. Rev. A* **66**, 898 (1972).
- [44] K. P. Huber and G. Herzberg, *Molecular Spectra and Molecular Structure IV: Constants of Diatomic Molecules* (Van Nostrand Reinhold, New York, 1979).
- [45] M. A. Morrison and P. J. Hay, *Phys. Rev. A* **20**, 740 (1979).
- [46] J. C. Light and R. B. Walker, *J. Chem. Phys.* **65**, 4272 (1976).
- [47] B. I. Schneider and R. B. Walker, *J. Chem. Phys.* **70**, 2466 (1979).
- [48] K. L. Baluja, P. G. Burke, and L. A. Morgan, *Comput. Phys. Commun.* **27**, 299 (1982).
- [49] L. A. Morgan, *Comput. Phys. Commun.* **31**, 419 (1984).
- [50] M. Gailitis, *J. Phys. B* **9**, 843 (1976).
- [51] C. J. Noble and R. K. Nesbet, *Comput. Phys. Commun.* **33**, 399 (1984).
- [52] R. K. Nesbet, *Comput. Phys. Commun.* **32**, 341 (1984).
- [53] M. A. Morrison, A. N. Feldt, and D. Austin, *Phys. Rev. A* **29**, 2518 (1984).
- [54] R. K. Nesbet, C. J. Noble, and L. A. Morgan, *Phys. Rev. A* **34**, 2798 (1986).
- [55] F. H. M. Faisal and A. Temkin, *Phys. Rev. Lett.* **28**, 203 (1972).
- [56] M. A. Morrison, A. N. Feldt, and B. C. Saha, *Phys. Rev. A* **30**, 2811 (1984).
- [57] B. I. Schneider, *Phys. Rev. A* **14**, 1923 (1976).